2022 Hunga-Tonga eruption: stratospheric aerosol evolution in a water-rich plume

Yunqian Zhu (yunqian.zhu@colorado.edu)
University of Colorado Boulder https://orcid.org/0000-0001-7751-397X

Charles Bardeen
National Center for Atmospheric Research

Simone Tilmes
National Center for Atmospheric Research

Michael Mills
NCAR https://orcid.org/0000-0002-8054-1346

V. Harvey
Laboratory for Atmospheric and Space Physics

Ghassan Taha
GESTAR II, Morgan State University

Douglas Kinnison
National Center for Atmospheric Research

Pengfei Yu
Jinan University

Karen Rosenlof
NOAA https://orcid.org/0000-0002-0903-8270

Xinyue Wang
National Center for Atmospheric Research

Melody Avery
NASA Langley Research Center

Corinna Kloss
Laboratoire de Physique de l'Environnement et de l'Espace, CNRS UMR 7328, Université d'Orléans

Can Li
NASA/Goddard Space Flight Center

Anne Glanville
National Center for Atmospheric Research

Luis Millán
NASA Jet Propulsion Laboratory

T Deshler
Univ Wyoming

Robert Portmann

NOAA Earth System Research Laboratory

Nickolay Krotkov

NASA Goddard Space Flight Center https://orcid.org/0000-0001-6170-6750

Owen Toon

University of Colorado Boulder

Article

Keywords:

Posted Date: May 12th, 2022

DOI: https://doi.org/10.21203/rs.3.rs-1647643/v1

Version of Record: A version of this preprint was published at Communications Earth & Environment on October 22nd, 2022. See the published version at https://doi.org/10.1038/s43247-022-00580-w.

Abstract

The January 2022 Hunga Tonga-Hunga Ha'apai (HTHH) volcanic eruption injected a relatively small amount of SO_2, but significantly more water into the stratosphere than previously seen in the modern satellite record. Here we show that the large amount of water resulted in large perturbations to stratospheric aerosol evolution. Our Community Earth System Model simulation reproduces the enhanced water vapor observed by the Microwave Limb Sounder at pressure levels between 10 and 50 hPa for three months. Compared with a simulation without a water injection, this additional source of water vapor increases OH, which halves the SO_2 lifetime. Subsequent coagulation creates larger sulfate particles that double the stratospheric aerosol optical depth. A seasonal forecast of volcanic plume transport in the southern hemisphere indicates this eruption will greatly enhance the aerosol surface area and water vapor near the polar vortex until at least October 2022, suggesting that there will continue to be an impact of the HTHH eruption on the climate system.

Main

On January 13 and 15 of 2022, the Hunga Tonga-Hunga Ha'apai (HTHH) submarine volcano (21°S, 175°W) erupted and injected volcanic material into the stratosphere up to an altitude of 58 km [1–3]. Observations from several satellites showed enhanced levels of stratospheric sulfur dioxide (SO2) (by TROPOMI and OMPS-NM), water vapor (by MLS), aerosols (by OMPS and CALIPSO), and possibly ice (by CALIPSO) as we will discuss in this work. Unlike some land-based volcanos, HTHH injected more than 100 Tg of water into the stratosphere[4], which normally contains about 1500 Tg of water globally for a typical tropopause pressure of 100 hPa. The Microwave Limb Sounder (MLS) onboard NASA's Earth Observing System (EOS) Aura satellite[5] observed enhanced water vapor that persisted for more than three months. The Cloud-Aerosol Lidar with Orthogonal Polarization (CALIOP) on the Cloud-Aerosol Lidar and Infrared Pathfinder Satellite Observation (CALIPSO) satellite[6] observed two distinct aerosol types on January 16 after the eruption: one with weak 532 nm depolarization indicating spherical particles (such as sulfate aerosol) above 20 km, and layers at lower altitudes with large depolarization indicating particles with nonspherical shapes (such as volcanic ash and ice) (Figure S1). It is typical to see ice and ash immediately after an eruption (i.e. [7]). However, it is surprising to see abundant sulfate aerosol with large extinction/backscatter coefficients so quickly, because SO_2 takes time to be oxidized and for H_2SO_4 to nucleate into sulfate aerosol[8].

Stratospheric water vapor and volcanic aerosols are important to both chemistry[9–13] and radiative balance[14–17]. Here, we demonstrate that enhanced H_2O promotes faster sulfate aerosol formation in the stratosphere leading to larger particles and larger aerosol optical depth. The water vapor injection and a small amount of evaporating ice deposits substantial water vapor in the stratosphere (Results 1). Large water vapor abundances result in the formation of OH which acts to speed up the conversion of SO_2 to H_2SO_4 (Results 2). Because of the faster formation and coagulation of sulfate aerosol, particles form with larger sizes and hence larger extinction than the ones without water injection (Results 3). Finally, we

predict the water vapor and aerosols that get transported toward the South Pole will linger near the polar vortex until at least October 2022 (Results 4).

Results

1. Both water injection and evaporating ice determine the water vapor remaining in the stratosphere

Here we use the Whole Atmosphere Community Climate Model (WACCM) to simulate the persistent water vapor enhancement from 10 to 50 hPa observed by MLS version 4 (Figure 1a) from February to April. Zonal averages of simulated water vapor on March 1 shows good agreement with MLS observations (Figure S2). Figure 1a shows both the model (solid line) and MLS (dashed line) display a positive water vapor anomaly of 6 - 8 ppmv peaking at 30 hPa from February to April. The anomaly is averaged from 30˚S to 0˚ and calculated using February, March, and April profiles minus the profile on January 5. The simulation has wider vertical extent in March and April. Both the model and MLS (Figure 1a) show that the positive water vapor anomaly slowly ascends from February 10 to April 1, which is largely related to the ascending branch of Brewer-Dobson circulation [18](Figure S2b).

To be consistent with the MLS water anomalies[4], we need to inject ~ 150 Tg of water in an area of ~ 710^5 km^2, which is about three times larger than the anvil size observed by NOAA's Geostationary Operational Environmental Satellite 17 on January 15, 2022. This large area is needed because the residual amount of water is determined by the ice vapor pressure curve as shown in Figure S3. If we inject the water into a smaller area, the model forms too much ice and cannot retain enough water at 30 hPa as observed. It is not unreasonable to inject in a larger area. MLS observations on Jan 16 (a day after the eruption) show the latitudinal spreading of water vapor anomaly is more than 10 degrees[4]. The simulated plume does not spread as fast as observed because it is hard for the global model to reproduce the vertical wind shear as observed due to the limited spatial resolution, especially for a tropical volcanic plume spreading in the first couple of days[19]. In the model, the injection is over 6 hours on January 15, 2022 between 25.5 km and 35 km with a majority of the water injected between 25.5 and 30 km (see methods for details). The model simulation (Figure 1b) shows that 10 Tg of ice falls out and 10 Tg of ice evaporates and contributes to the residual water vapor (~140 Tg) until April. In reality, it is possible more H_2O was injected to form ice but these ice particles fell out because of their large sizes or forming aggregates with ash particles[7].

2. The water injection significantly shortens the SO_2 lifetime by providing abundant OH

An accurate volcanic SO_2 lifetime is key for predicting the particle sizes in the volcanic cloud. With shorter lifetimes, the resulting aerosol concentration is higher, leading to more rapid coagulation and larger sulfate particles[20]. In the stratosphere, the volcanic SO_2 lifetime is mainly determined by its reaction rate with OH, as well as the heterogeneous reaction on ash[19]. The depletion of OH in SO_2-rich plumes slows the SO_2/OH reaction[8,19,21–23]. However, during the HTHH eruption, the significant amount of water vapor injected rapidly increased OH (Figure S4) and shortened the SO_2 lifetime as shown in Figure 2. Clegg & Abbatt[24] demonstrated that SO_2 uptake on the ice surfaces is insignificant, so this mechanism is not included in the model. The SO_2 lifetime (the e-folding time) of the SO2only case (red line) is 28 days, while the SO_2 lifetime of the SO2_H2O case (blue solid line) is 12 days. Zhu et al.[19] showed that a considerable amount of SO_2 might be undetectable because it falls below the detection limits of the instruments as it spreads through the atmosphere. However, the blue dashed line in Figure 2 suggests that this effect is small for this eruption for the first ten days.

3. The impact of enhanced water vapor on stratospheric aerosol optical depth and radiation

We compare the stratospheric aerosol optical depth (sAOD) between OMPS-LP data and two model cases in Figure 3. Without the water injection, the SO2only case has a very small sAOD in the first two weeks after the eruption, because SO_2 converts slowly to H_2SO_4 with a lifetime of ~1 month (Figure 2). Both OMPS and the SO2_H2O case show almost immediate formation of a large amount of sulfate aerosol. OMPS LP sAOD retrieval during the first couple of days has large uncertainties when the volcanic clouds are optically thick and localized[26]. The backscatter coefficient at visible wavelengths for the SO2_H2O case and CALIOP shows a similar peak value of 0.005 to 0.01 $km^{-1}sr^{-1}$ (Figure S5). In addition, compared to the SO2only case, sulfate particles in the SO2_H2O case doubled the sAOD in February because sulfate forms faster in the SO2_H2O case, and the more abundant particles coagulate to larger sizes. Also, sulfate particles swell to be a little larger because of the enhanced background water vapor (Figure S6). Generally, OMPS-LP observes a faster spreading of the plume to the northern hemisphere than is simulated (Figure 3) and has higher optic values in the northern hemisphere in March (Figure S7). Sellitto et al.[27] indicate the initial fast spreading of the HTHH aerosol plume is highly related to the strong cooling inside the plume. Our model is nudged to the observed meteorology, which doesn't capture this strong local cooling. Also, as we discuss in Result 1, the global model cannot reproduce the vertical wind shear as observed due to the limited spatial resolution. On March 1, the SO2_H2O case and the OMPS observation are consistent regarding the vertical extent of the plume from 20-30 km, and the extension to 40˚S (Figure S7).

Because of the increase in the burden of sulfate, the volcanic plume creates a negative radiative effect of about -1 to -2 W/m^2 in the perturbed areas in January and February (Figure 4). The global mean radiative effect at the top of the atmosphere in February is -0.12 W/m^2 in the SO2only case and -0.20 W/m^2 in the

SO2_H2O case; the surface radiative effect is -0.16 W/m^2 for the SO2only case and -0.21 W/m^2 for the SO2_H2O case. These values are typical for middle-sized volcanic eruptions[28]. Even though the sAOD is approximately doubled in the SO2_H2O case, it only results in slightly more negative radiative forcing due to enhanced positive radiative forcing of the enhanced water vapor [29,30] in the SO2_H2O case.

4. Persistent volcanic water vapor and sulfate may impact stratospheric ozone chemistry

Here we focus our study on the transport of volcanic water vapor and sulfate in the Southern Hemisphere. We conduct three sets of 3-member ensemble simulations to explore the transport of volcanic water vapor and volcanic sulfur from January to October. The simulations are nudged to the observed meteorology until the end of March and then are free-running until October. Figure 5 shows that both H_2O and sulfur are slowly transported to the south from January to May. After mid-June, the majority of H_2O and sulfur reside between 30˚S and 60˚S. This is because the strong Antarctic vortex during June-July-August prevents volcanic materials from entering the polar cap. The black contours in Figure 5 are the zonal wind showing the polar vortex starts to build up in April and remains through October between 50˚S and 60˚S. Figures 5c and 5d show the percentage increase compared to the background levels of H_2O and sulfur. Even though the majority of volcanic material is outside the polar vortex, we see a ~10% increase of sulfur at 90˚S starting from April and the sulfur mass almost doubles in October. The sulfate aerosol provides extra surface area density (SAD) for heterogeneous reactions affecting ozone chemistry. On the other hand, water increases by about 30% at the edge of the vortex (~ 60˚S) after June. However, due to polar stratospheric cloud formation and dehydration, the positive water anomaly inside the polar vortex does not pass the Student's t-test at a 90% significance level.

The simulations predict an increase in water vapor and aerosol surface area density (SAD) near the vortex. These changes are expected to impact polar ozone because heterogeneous reactions on polar stratospheric clouds and volcanic particles convert inactive chlorine ($ClONO_2$ and HCl) into photochemically active chlorine[31,32]. Figures 6a and 6b show that water increases by about 2-3 ppmv and SAD increases by about 2 to 4 μm^2/cm^3 near the edge of the vortex by the end of September. Water vapor increases between 50 to 10 hPa, while the aerosol increase is between 150 hPa to 30 hPa. This difference in altitude occurs because of aerosol sedimentation during transport. Figure 6c shows the HCl+$ClONO_2$ heterogeneous reaction rate as a function of temperature for different amounts of water vapor. The reaction probability increases about one order of magnitude as we increase water by 3 ppmv above 194 K.

Discussion

The HTHH eruption provides a natural testbed to show how increased water vapor in the stratosphere can impact the Earth system. This work demonstrates the importance of the water vapor injection on aerosol

and aerosol-related chemistry using a state-of-the-art global climate model. The simulation shows that water vapor significantly shortens the SO_2 lifetime and doubles aerosol extinction relative to the simulation with only an SO_2 injection. The global radiative forcing of HHTH is on the order of -0.1 to -0.2 W/m^2 though it is about -1 to -2 W/m^2 from 30˚S to 0˚ during the two months after the eruption. In the forecast simulation, volcanic water and sulfate persist near the polar vortex until at least October 2022. The model developed here provides opportunities for future studies on the climate impact, and effects on ozone, of HTHH eruption as it continues to evolve.

Online Methods

1. Model setup

We utilize the Community Earth System Model version 2 (CESM2) with the Whole Atmosphere Community Climate Model (WACCM)[33] using 70 layers extending upward to 140 km. The vertical resolution is about 1 to 1.5 km in the stratosphere. The model is fully coupled to an interactive ocean, sea-ice, and land. The ocean and sea-ice are initialized on January 3 with output from a stand-alone ocean model forced by atmospheric state fields and fluxes from the Japanese 55-year Reanalysis. Likewise, the land is initialized with output from a stand-alone land model forced with atmospheric data from the National Center for Environmental Prediction Climate Forecast System, version 2. These are the same initializations that were used in the subseasonal-to-seasonal project outlined in Richter et al.[34]. The atmosphere is initialized from a transient WACCM simulation[33]. Between January 3 and March 30, 2022, the atmospheric component is nudged to GEOS5 meteorological analysis[35] with a 12-hour relaxation using 3-hour meteorology[36]. After April 1, three ensemble members with a fully interactive atmosphere and ocean are continued into the future until the end of October. The three ensemble members differ in the last date of nudging (namely March 29, 30, and 31). We conducted three sets of ensemble members: the control case without SO_2 or H_2O; the SO2only case with only SO_2 injection; and the SO2_H2O case with both SO_2 and H_2O injection.

The SO_2 injection amount is based on the TROPOMI and OMPS Nadir Mapper (NM) SO_2 [37] reported at https://so2.gsfc.nasa.gov/. We tune the SO_2 injection vertical distributions based on comparisons between the simulated sulfate aerosol and OMPS LP aerosol extinction in March (i.e., Figure S7). We tune the H_2O injection amount and vertical distribution mainly to retain enough H_2O between 10 and 50 hPa as seen by MLS in Feb, March, and April (i.e., Figure 1a). MLS also sees a small amount of water between 10 to 1 hPa in those days[4]. We inject 0.42 Tg of SO_2 and 150 Tg of H_2O from 4 UTC to 10 UTC on January 15, 2022 (ignoring the small eruption that occurred on January 13, 2022. Note that this small eruption also put ice into the lower stratosphere, up to 20 km). The vertical distribution of SO_2 is 0.3 Tg from 20 km to 22 km and 0.12 Tg from 22-28 km with constant concentrations in these layers. The vertical distribution of H_2O is 103 Tg from 25.5-27 km, 42 Tg from 27-30 km, and 5 Tg from 30-35 km with constant concentration. We inject the plume into an area of ~ 710^5 km^2 between 22˚S-14˚S and

182˚E-186˚E, which is about three times larger than the anvil size observed by NOAA's Geostationary Operational Environmental Satellite 17 on January 15, 2022. This is because the global model cannot spread the plume as fast as observed as we discuss in Result 1 and Result 3. We haven't considered ash injection since satellite observations (e.g., OMPS measured low UV Aerosol Index) don't show evidence of significant ash persisting for a long time. CALIOP sees that the majority of the high backscatter coefficient above 20 km correlates with low depolarization indicating the composition is mainly spherical sulfate particles. The Light Optical Aerosol Counter (LOAC) measurements at Reunion island (21.1˚S, 55.3˚E) on January 23 and January 26 mainly see submicron particles indicating no large volcanic ash or other large (> 1 μm) volcanic particles present.

For ice cloud formation, we modified the nucleation parameterization to allow both homogeneous freezing and heterogeneous nucleation to occur in the stratosphere when temperatures are cold (< -40 °C).

2. Observations

The MLS instrument onboard the EOS Aura satellite was launched into a near-polar sun-synchronous orbit in 2004 and measures atmospheric composition, temperature, humidity, and cloud ice. After the HTHH eruption, MLS detected enhanced water vapor. Here we use MLS version 4 quality screened data[5] and do not use MLS ice water content as recommended by Millán et al.[4].

The OMPS Limb Profiler (LP)[38] data have been processed to create an aerosol extinction coefficient product from measurements of the limb scattered solar radiation at six wavelengths. The sensor employs three vertical slits separated horizontally. This work uses the version 2.0 OMPS aerosol extinction coefficient product at 997 nm wavelength[39] with relative accuracies and precisions close to 15%. We use the center slit aerosol retrieval because it has the most accurate radiometric calibration and stray light corrections[40].

SO_2 mass estimates from OMPS-NM are based on the NASA standard SNPP/OMPS SO_2 vertical column density (VCD) product, retrieved using a principal component analysis (PCA) spectral fitting algorithm[37] assuming a fixed a priori profile centered at 18 km altitude. The estimated uncertainty of ~35% (error bar in Figure 2) reflects potential errors that can be caused by the highly unusual injection height and the large amounts of aerosols and ice particles for the HTHH eruption.

Declarations

Acknowledgment

The work at the University of Colorado Boulder was supported by NASA grant 80NSSC19K1276. This project received funding from NOAA's Earth Radiation Budget (ERB) Initiative (CPO #03-01-07-001). CK

acknowledges the support by LABEX-VOLTAIRE (ANR-10-LABEX-100-01). PY is supported by the National Natural Science Foundation of China (42175089, 42121004). Development, analysis, and maintenance of the OMPS-NM SO_2 product are supported by the NASA Earth Science TASNPP (grant # 80NSSC18K0688) and SNPPSP (grant # 80NSSC22K0158) programs. Development, analysis, and maintenance of the OMPS-LP aerosol product are supported by the NASA Earth Science TASNPP (grant # 80NSSC18K0847) and SNPPSP (grant # 80NSSC22K0157) programs. We thank the discussions at the SSiRC volcano forum led by Dr. Jean-Paul Vernier. We thank Dr. Nathaniel Livesey and Dr. Michelle Santee from the NASA MLS team, Dr. Margaret Tolbert from CU Boulder, Dr. Jadwiga Richter, Dr. William Randel and Dr. Mijeong Park from NCAR, Dr. Peter Colarco from NASA Goddard, Dr. Michael Pitts from NASA Langley, Dr. Ming Deng from LASP, and Dr. Tao Wang from NASA JPL, for their valuable input. NCAR's Community Earth System Model is supported by NSF and the Office of Science of the U.S. Department of Energy. We acknowledge high-performance computing support from Cheyenne (doi:10.5065/ D6RX99HX) provided by NCAR's Computational and Information Systems Laboratory (CISL), sponsored by the NSF.

References

1. Carr, J. L., Horváth, Á., Wu, D. L. & Friberg, M. D. Stereo Plume Height and Motion Retrievals for the Record-Setting Hunga Tonga-Hunga Ha'apai Eruption of 15 January 2022. Geophysical Research Letters e2022GL098131 (2022).
2. Proud, S. R., Prata, A. & Schmauss, S. The January 2022 eruption of Hunga Tonga-Hunga Ha'apai volcano reached the mesosphere. (2022).
3. Yuen, D. A. *et al.* Under the surface: Pressure-induced planetary-scale waves, volcanic lightning, and gaseous clouds caused by the submarine eruption of Hunga Tonga-Hunga Ha'apai volcano. Earthquake Research Advances 100134 (2022).
4. Millán, L. *et al.* Hunga Tonga-Hunga Ha'apai Hydration of the Stratosphere. Preprint ESSOAr (2022) doi:doi.org/10.1002/essoar.10511266.1.
5. Livesey, N. J. *et al.* Version 4.2x Level 2 and 3 data quality and description document (Tech. Rep. No. JPL D-33509 Rev. E). (2020).
6. Winker, D. M., Hunt, W. H. & McGill, M. J. Initial performance assessment of CALIOP. Geophysical Research Letters **34**, (2007).
7. Guo, S., Rose, W. I., Bluth, G. J. S. & Watson, I. M. Particles in the great Pinatubo volcanic cloud of June 1991: The role of ice. Geochemistry, Geophysics, Geosystems **5**, (2004).
8. Mills, M. J. *et al.* Radiative and chemical response to interactive stratospheric sulfate aerosols in fully coupled CESM1(WACCM). Journal of Geophysical Research: Atmospheres **122**, 13,061 – 13,078 (2017).
9. Dvortsov, V. L. & Solomon, S. Response of the stratospheric temperatures and ozone to past and future increases in stratospheric humidity. Journal of Geophysical Research: Atmospheres **106**, 7505–7514 (2001).

10. Hofmann, D. & Oltmans, S. The effect of stratospheric water vapor on the heterogeneous reaction rate of ClONO2 and H2O for sulfuric acid aerosol. Geophysical research letters **19**, 2211–2214 (1992).
11. Solomon, S. Stratospheric ozone depletion: A review of concepts and history. Reviews of Geophysics **37**, 275–316 (1999).
12. Solomon, S. *et al.* Emergence of healing in the Antarctic ozone layer. Science **353**, 269–274 (2016).
13. Zhu, Y. *et al.* Stratospheric aerosols, Polar Stratospheric Clouds, and polar ozone depletion after the Mount Calbuco eruption in 2015. Journal of Geophysical Research: Atmospheres **123**, 12,308 – 12,331 (2018).
14. de F. Forster, P. M. & Shine, K. P. Stratospheric water vapour changes as a possible contributor to observed stratospheric cooling. Geophysical research letters **26**, 3309–3312 (1999).
15. Shindell, D. T. Climate and ozone response to increased stratospheric water vapor. Geophysical Research Letters **28**, 1551–1554 (2001).
16. Smith, C. A., Haigh, J. D. & Toumi, R. Radiative forcing due to trends in stratospheric water vapour. Geophysical research letters **28**, 179–182 (2001).
17. Solomon, S. *et al.* Contributions of stratospheric water vapor to decadal changes in the rate of global warming. Science **327**, 1219–1223 (2010).
18. Ploeger, F. *et al.* The stratospheric Brewer–Dobson circulation inferred from age of air in the ERA5 reanalysis. Atmospheric Chemistry and Physics **21**, 8393–8412 (2021).
19. Zhu, Y. *et al.* Persisting volcanic ash particles impact stratospheric SO2 lifetime and aerosol optical properties. Nature Communications **11**, 4526 (2020).
20. Clyne, M. *et al.* Model physics and chemistry causing intermodel disagreement within the VolMIP-Tambora Interactive Stratospheric Aerosol ensemble. *Atmos. Chem. Phys. Discuss.* 2020, 1–43 (2020).
21. Bekki, S. Oxidation of volcanic SO2: A sink for stratospheric OH and H2O. Geophysical Research Letters **22**, 913–916 (1995).
22. Pinto, J. P., Turco, R. P. & Toon, O. B. Self-limiting physical and chemical effects in volcanic eruption clouds. Journal of Geophysical Research: Atmospheres **94**, 11165–11174 (1989).
23. Savarino, J., Bekki, S., Cole-Dai, J. & Thiemens, M. H. Evidence from sulfate mass independent oxygen isotopic compositions of dramatic changes in atmospheric oxidation following massive volcanic eruptions. Journal of Geophysical Research: Atmospheres **108**, (2003).
24. Clegg, M. & Abbatt, D. Uptake of Gas-Phase SO2 and H2O2 by Ice Surfaces: Dependence on Partial Pressure, Temperature, and Surface Acidity. J. Phys. Chem. A **105**, 6630–6636 (2001).
25. Theys, N. *et al.* Sulfur dioxide retrievals from TROPOMI onboard Sentinel-5 Precursor: algorithm theoretical basis. Atmospheric Measurement Techniques **10**, 119–153 (2017).
26. DeLand, M. Readme document for the Soumi-NPP OPMS LP L2 AER675 Daily product. (2019).

27. Sellitto, P. *et al.* The unexpected radiative impact of the Hunga Tonga eruption of January 15th, 2022. (2022).
28. Schmidt, A. *et al.* Volcanic radiative forcing from 1979 to 2015. Journal of Geophysical Research: Atmospheres **123**, 12491–12508 (2018).
29. Huang, Y. On the longwave climate feedbacks. Journal of climate **26**, 7603–7610 (2013).
30. Dessler, A., Schoeberl, M., Wang, T., Davis, S. & Rosenlof, K. Stratospheric water vapor feedback. *Proceedings of the National Academy of Sciences* **110**, 18087–18091 (2013).
31. Solomon, S., Garcia, R. R., Rowland, F. S. & Wuebbles, D. J. On the depletion of Antarctic ozone. Nature **321**, 755–758 (1986).
32. Solomon, S. *et al.* The role of aerosol variations in anthropogenic ozone depletion at northern midlatitudes. Journal of Geophysical Research: Atmospheres **101**, 6713–6727 (1996).
33. Gettelman, A. *et al.* The Whole Atmosphere Community Climate Model Version 6 (WACCM6). Journal of Geophysical Research: Atmospheres **124**, 12380–12403 (2019).
34. Richter, J. H. *et al.* Subseasonal Earth system prediction with CESM2. Weather and Forecasting (2022).
35. Rienecker, M. M. *et al.* The GEOS-5 Data Assimilation System: Documentation of Versions 5.0. 1, 5.1. 0, and 5.2. 0. (2008).
36. Davis, N. A., Callaghan, P., Simpson, I. R. & Tilmes, S. Specified dynamics scheme impacts on wave-mean flow dynamics, convection, and tracer transport in CESM2 (WACCM6). Atmospheric Chemistry and Physics **22**, 197–214 (2022).
37. Li, C. *et al.* New-generation NASA Aura Ozone Monitoring Instrument (OMI) volcanic SO 2 dataset: Algorithm description, initial results, and continuation with the Suomi-NPP Ozone Mapping and Profiler Suite (OMPS). Atmospheric Measurement Techniques **10**, 445–458 (2017).
38. Flynn, L. E., Seftor, C. J., Larsen, J. C. & Xu, P. The ozone mapping and profiler suite. in *Earth science satellite remote sensing* 279–296 (Springer, 2006).
39. Taha, G. *et al.* OMPS LP Version 2.0 multi-wavelength aerosol extinction coefficient retrieval algorithm. *Atmos. Meas. Tech.* **14**, 1015–1036 (2021).
40. Jaross, G. *et al.* OMPS Limb Profiler instrument performance assessment. Journal of Geophysical Research: Atmospheres **119**, 4399–4412 (2014).
41. Goff, J. & Gratch, S. Low Pressure Properties of H2O From-120F to 212F. Heating, Piping and Air Conditioning **18**, 125–136 (1946).
42. Jäger, H. & Deshler, T. Lidar backscatter to extinction, mass and area conversions for stratospheric aerosols based on midlatitude balloonborne size distribution measurements. Geophysical Research Letters **29**, 35–1 (2002).
43. Jäger, H. & Deshler, T. Correction to “Lidar backscatter to extinction, mass and area conversions for stratospheric aerosols based on midlatitude balloonborne size distribution measurements”. Geophys. Res. Lett **30**, 1382 (2003).

44. Prata, A. T., Young, S. A., Siems, S. T. & Manton, M. J. Lidar ratios of stratospheric volcanic ash and sulfate aerosols retrieved from CALIOP measurements. Atmospheric Chemistry and Physics **17**, 8599–8618 (2017).

Figures

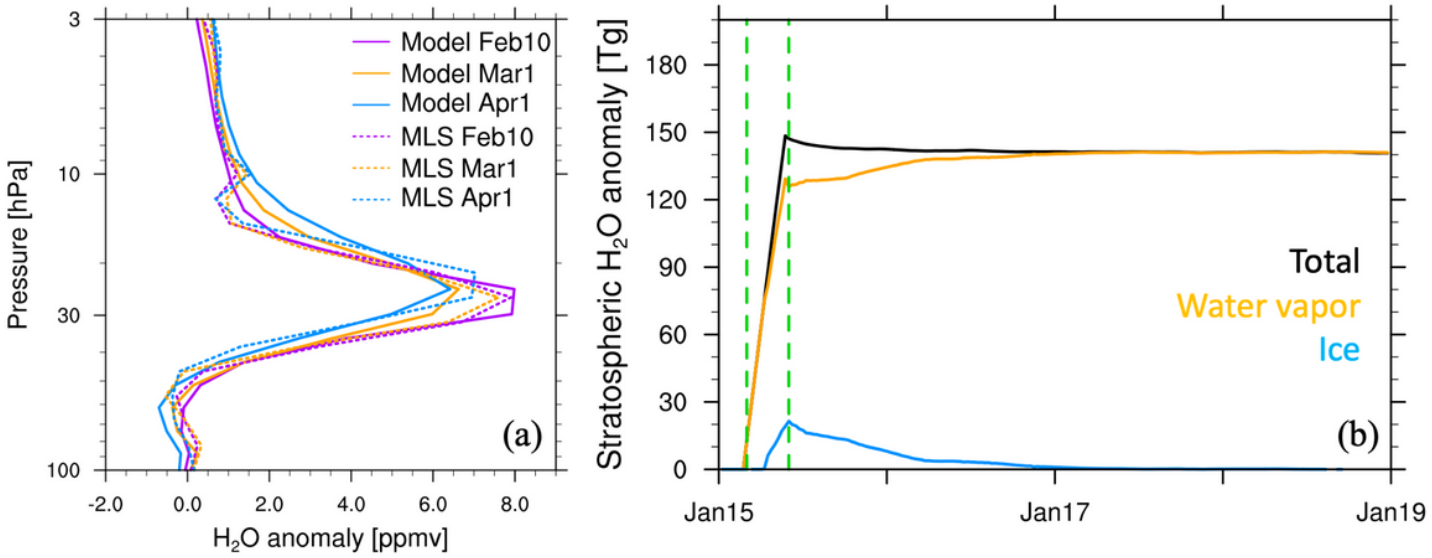

Figure 1

a). The zonal average H_2O anomaly profiles between 30˚S-0˚ on February 10, March 1, and April 1, 2022. The solid lines are simulations and the dashed lines are the MLS observations. The simulation and MLS anomaly curves are calculated using February, March, and April profiles minus the profile on January 5. b) Simulated stratospheric H_2O anomaly evolution in the first week. It is calculated using a case with H_2O injection minus a case without H_2O injection. The blue line is the ice, the orange line is the water vapor, and the black line is the total water. The green dashed lines indicate the water injection period.

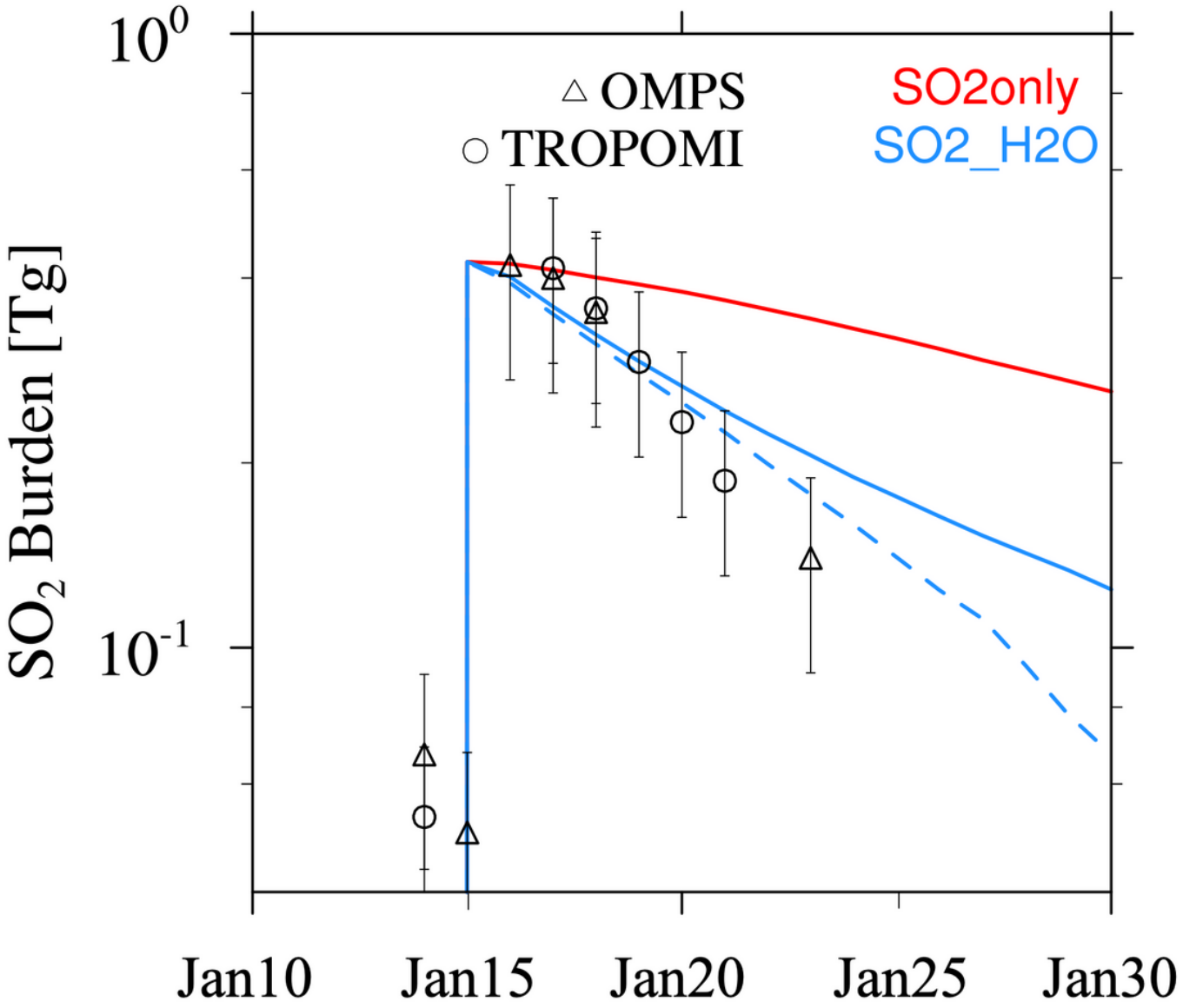

Figure 2

The time series of the stratospheric SO_2 burden from two model cases with (blue) and without (red) water injection. The dashed blue line is the SO2_H2O case excluding the SO_2 below 0.2 DU (i.e., the approximate OMPS-NM SO_2 detection limit). The circles and triangles are SO_2 measurements by OMPS-NM and TROPOMI. The error bars imply an estimated uncertainty of 35% and 30%[25] for OMPS-NM and TROPOMI SO_2 mass estimates, respectively. The observational data are from https://so2.gsfc.nasa.gov/. The SO2only run has the SO_2 injection; the SO2_H2O run has both the SO_2 and H_2O injections (detailed in Online methods).

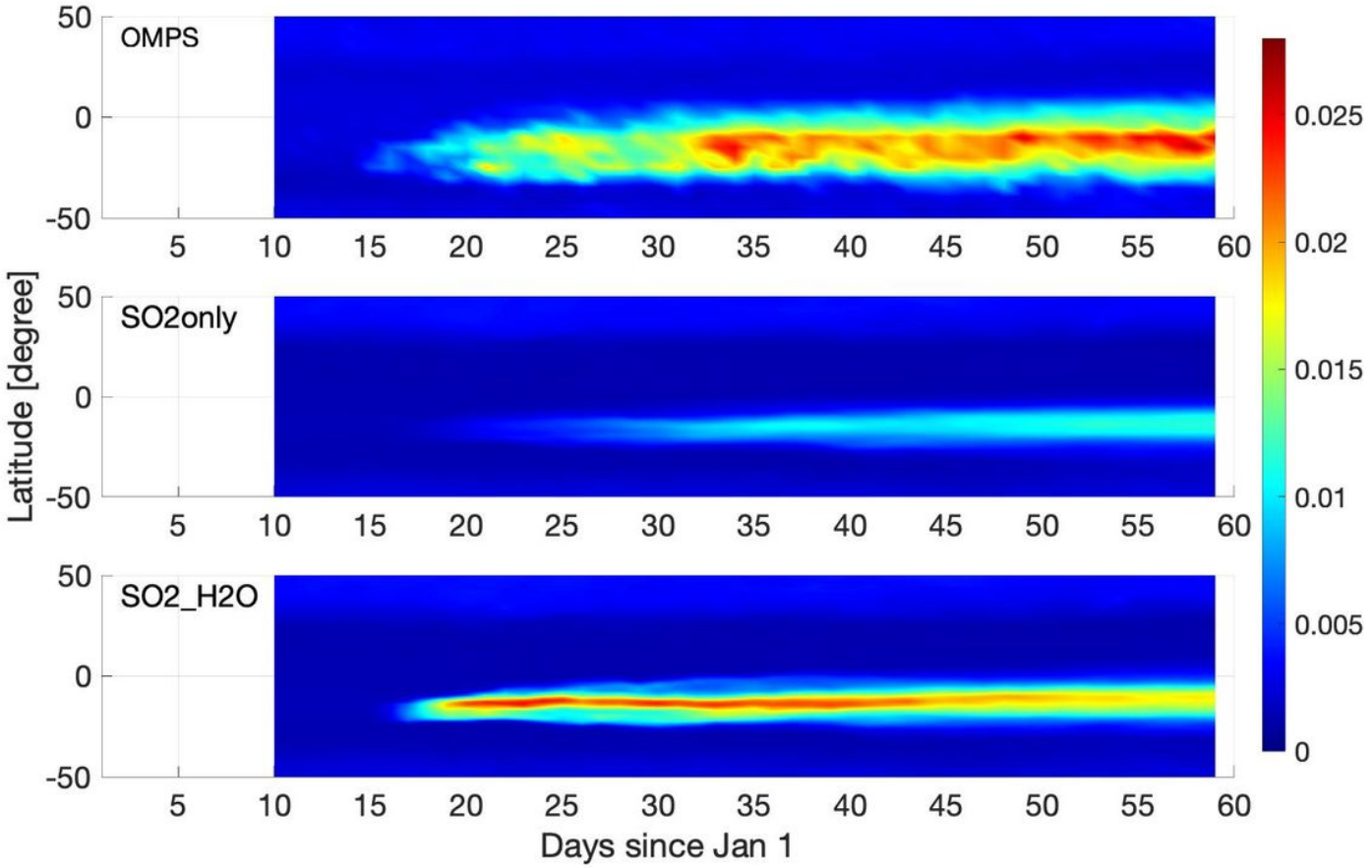

Figure 3

The zonal mean column sAOD (background aerosol+volcanic aerosol) from OMPS LP at 997 nm (top) and the simulated near-infrared sAODs for cases without (middle, the SO2only case) and with the water injection (bottom, the SO2_H2O case).

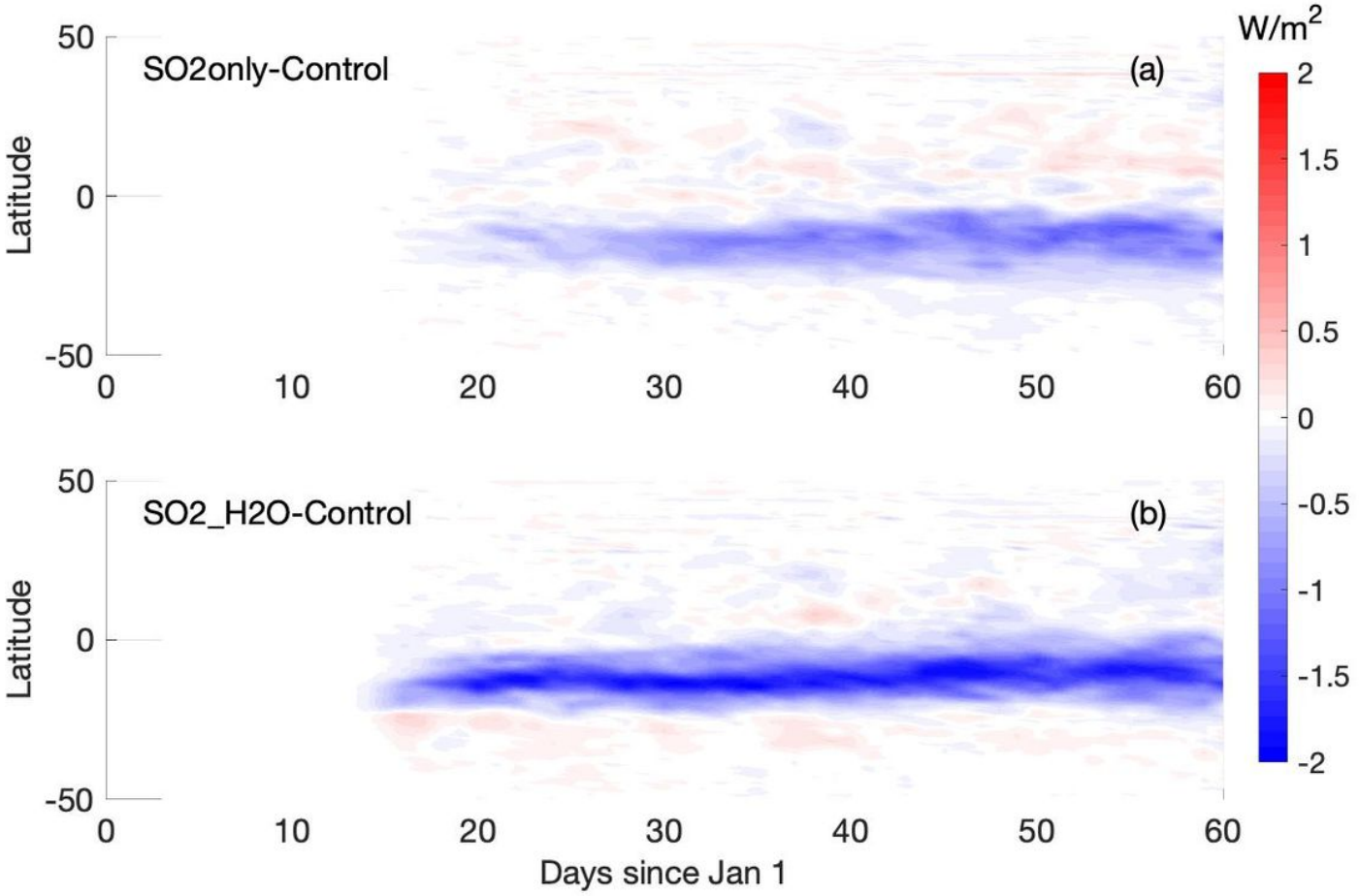

Figure 4

The zonal average aerosol radiative effect of the top of the atmosphere from January to March 2022 for the SO2only case (a) and the SO2_H2O case (b).

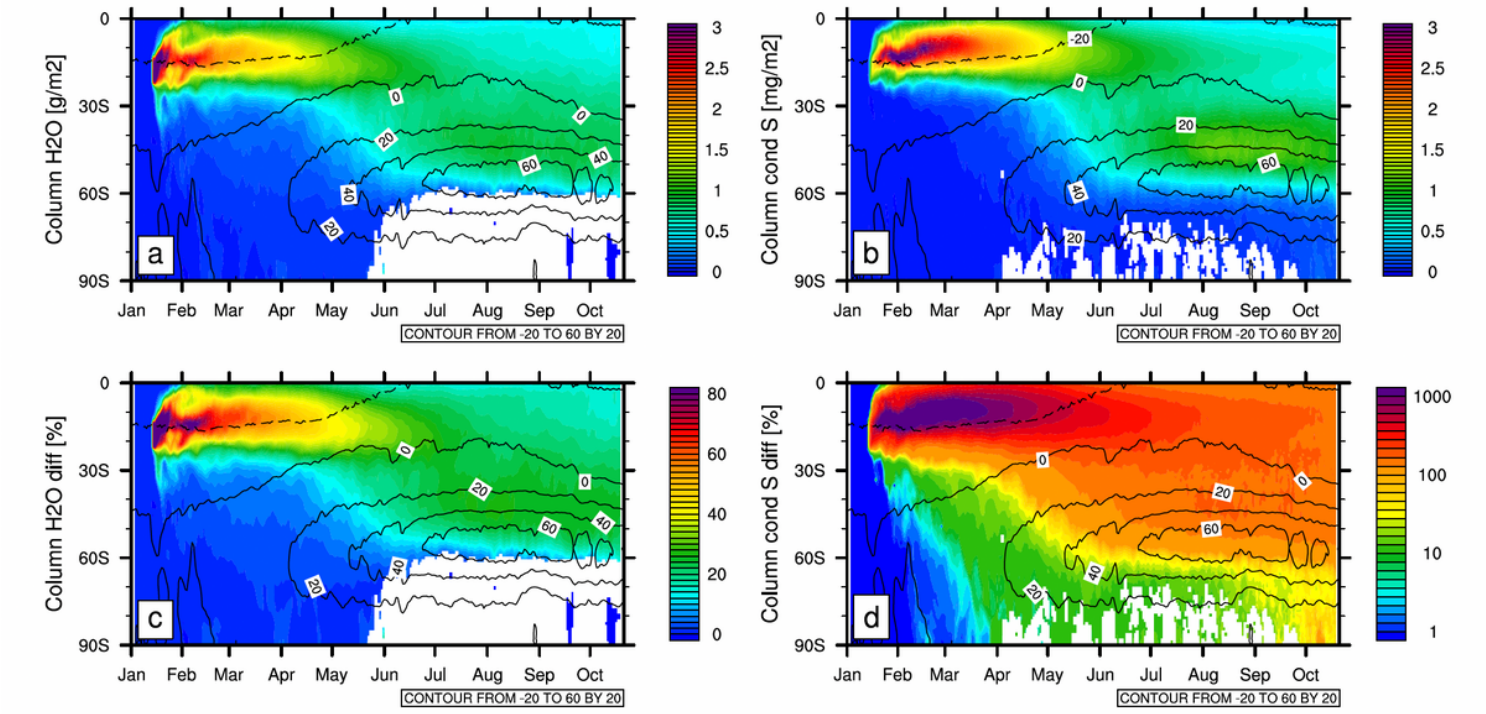

Figure 5

Panels a and b: the transport of volcanic column H_2O and volcanic column sulfur mass densities towards the South Pole. “Column cond S” means the sulfur in the condensed phase. Panel c and d: similar but plotted as the percentage increase relative to background H_2O and sulfur. After April 1, white areas mean the anomaly is not significant using the t-test at a 90% confidence level based on three ensemble members after April 1, 2022. The contours are the zonal wind showing the polar vortex from April to October at around 60˚S.

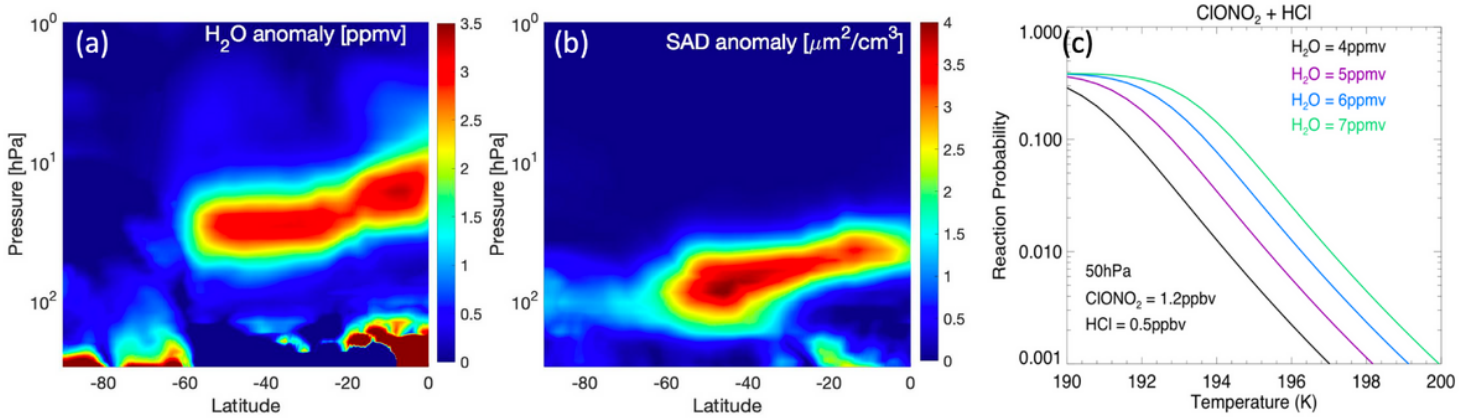

Figure 6

The simulated water vapor anomaly (a) and the aerosol SAD anomaly (b) in late September. These anomalies are calculated using the SO2_H2O case minus the control case. (c) The heterogeneous reaction rate as a function of water vapor assuming 0.1 μm particle size.

Supplementary Files

This is a list of supplementary files associated with this preprint. Click to download.

- Supplementary.docx